

# Spontaneous fission of the superheavy nucleus $^{286}\text{Fl}$

D. N. Poenaru\* and R. A. Gherghescu\*

*Horia Hulubei National Institute of Physics and Nuclear Engineering (IFIN-HH),*

*P.O. Box MG-6, RO-077125 Bucharest-Magurele, Romania and*

*Frankfurt Institute for Advanced Studies,*

*Johann Wolfgang Goethe University, Ruth-Moufang-Str. 1,*

*D-60438 Frankfurt am Main, Germany*

(Dated: )

## Abstract

The decimal logarithm of spontaneous fission half-life of the superheavy nucleus  $^{286}\text{Fl}$  experimentally determined is  $\log_{10} T_f^{\text{exp}}(s) = -0.632$ . We present a method to calculate the half-life based on the cranking inertia and the deformation energy, functions of two independent surface coordinates, using the best asymmetric two center shell model. Spherical shapes are assumed. In the first stage we study the statics. At a given mass asymmetry up to about  $\eta = 0.5$  the potential barrier has a two hump shape, but for larger  $\eta$  it has only one hump. The touching point deformation energy versus mass asymmetry shows the three minima, produced by shell effects, corresponding to three decay modes: spontaneous fission, cluster decay, and  $\alpha$  decay. The least action trajectory is determined in the plane  $(R, \eta)$ , where  $R$  is the separation distance of the fission fragments and  $\eta$  is the mass asymmetry. We may find a sequence of several trajectories one of which gives the least action. The parametrization with two deformation coordinates  $(R, \eta)$  and the radius of the light fragment,  $R_2$ , exponentially or linearly decreasing with  $R$  is compared with the simpler one, in which  $R_2 = \text{constant}$  and with a linearly decreasing or linearly increasing  $R_2$ . The latter is closer to the reality and reminds us about the  $\alpha$  or cluster preformation at the nuclear surface.

PACS numbers: 25.85.Ca, 24.75.+i, 21.10.Tg, 27.90.+b

---

\* poenaru@fias.uni-frankfurt.de

## I. INTRODUCTION

Superheavy (SH) nuclei, with atomic numbers  $Z = 104 - 118$ , are decaying mainly by  $\alpha$  decay and spontaneous fission. They have been produced in cold fusion or hot fusion ( $^{48}\text{Ca}$  projectile) reactions [1–10]. In a systematic study of  $\alpha$ -decay energies and half-lives of superheavy nuclei it was shown [11] that our semFIS (semiempirical formula based on fission theory) and UNIV (universal curve) are the best among 18 calculations methods of  $\alpha$  decay half-lives. For some isotopes of even heavier SHs, with  $Z > 121$ , there is a good chance for cluster decay modes to compete [12, 13].

There are many sources of experimental values for half-lives,  $T_f$ , of SHs against spontaneous fission, e.g., [14]. Among them we found  $\log_{10} T_f^{exp}(s) = -3.086, -0.980$  for  $^{282,284}\text{Cn}$  and  $-0.632$  for  $^{286}\text{Fl}$ . Calculations have been also performed with different models [15–22].

Fission dynamics with Werner-Wheeler nuclear inertia tensor [23] is not leading closer to experiment due to a too small value of inertia; we tried to improve the agreement between theory and experiment for  $^{284}\text{Cn}$  by using different laws of variation of mass parameter with fragment separation distance. Better results are obtained for  $^{282}\text{Cn}$  with cranking inertia [24] by assuming the most effective split to be  $^{282}\text{Cn} \rightarrow ^{130}\text{Pd} + ^{152}\text{Dy}$ .

In the present work we continue to use the cranking inertia [25–27] introduced by Inglis [28]. This time we try to find out the least action trajectory in the plane of two independent variables  $(R, \eta)$ , where  $R$  is the separation distance of the fragments and  $\eta = (A_1 - A_2)/A$  is the mass asymmetry with  $A, A_1, A_2$  the mass numbers of the parent and nuclear fragments. We assume  $A_1 \geq A_2$  hence  $\eta \geq 0$ . Consequently both potential energy surfaces and contour plots (figures like Figs. 1, 3, 7), function of  $(R, \eta)$ , will not have the mirror part corresponding to  $A_1 < A_2$ .

There are two main terms in the action integral allowing to calculate the half-life: the total deformation energy and the cranking inertia, both functions of  $(R, \eta)$ . We are using the macroscopic-microscopic method [29] to estimate the deformation energy, expressed as a sum of Yukawa-plus-exponential (Y+EM) [30] phenomenological energy,  $E_{Y+E}$ , and the shell plus pairing corrections,  $\delta E = \delta U + \delta P$  based on the asymmetric two center shell model (ATCSM) [31, 32]:

$$E_{def} = E_{Y+E} + \delta E \tag{1}$$

We shall briefly outline the model and discuss the obtained results.

## II. MODEL

### A. Surface parametrization. Two deformation parameters

By choosing four independent deformation parameters  $R, b_2, \chi_1, \chi_2$  [33] during the deformation from one parent nucleus to two fission fragments, the surface equation in cylindrical coordinates  $\rho, z$  is given by

$$\rho_s^2(z; b_1, \chi_1, b_2, \chi_2) = \begin{cases} b_1^2 - \chi_1^2 z^2 & , -a_1 < z < z_c \\ b_2^2 - \chi_2^2 (z - R)^2 & , z_c < z < R + a_2 \end{cases} \quad (2)$$

where  $z_c$  is the position of the crossing plane.

The semiaxes ratio of spheroidally deformed fragments are denoted by  $\chi_1 = b_1/a_1$ ,  $\chi_2 = b_2/a_2$ . The scalar,  $B(R)$ , is determined by the components of the nuclear inertia tensor and the derivatives with respect to  $R$ :

$$\begin{aligned} B(R) = & B_{b_2 b_2} \left( \frac{db_2}{dR} \right)^2 + 2B_{b_2 \chi_1} \frac{db_2}{dR} \frac{d\chi_1}{dR} + 2B_{b_2 \chi_2} \frac{db_2}{dR} \frac{d\chi_2}{dR} + \\ & 2B_{b_2 R} \frac{db_2}{dR} + B_{\chi_1 \chi_1} \left( \frac{d\chi_1}{dR} \right)^2 + 2B_{\chi_1 \chi_2} \frac{d\chi_1}{dR} \frac{d\chi_2}{dR} + \\ & 2B_{\chi_1 R} \frac{d\chi_1}{dR} + B_{\chi_2 \chi_2} \left( \frac{d\chi_2}{dR} \right)^2 + 2B_{\chi_2 R} \frac{d\chi_2}{dR} + B_{RR} \end{aligned} \quad (3)$$

When the two fragments are spheres,  $b_2 = R_2$ ,  $\chi_1, \chi_2 = 1$ , meaning that  $\frac{d\chi_1}{dR} = \frac{d\chi_2}{dR} = 0$  and the above equation becomes

$$B(R) = B_{b_2 b_2} \left( \frac{db_2}{dR} \right)^2 + 2B_{b_2 R} \frac{db_2}{dR} + B_{RR} = B_{22} + B_{21} + B_{11} \quad (4)$$

The derivative  $\frac{db_2}{dR} = \frac{dR_2}{dR}$  depends only on geometry. It is a negative quantity since  $R_2$  decreases exponentially with  $R$ ; its absolute values are rather small.

For a given mass asymmetry the final value of the radius of the light fragment  $R_{2f} = r_0 A_2^{1/3}$  is well determined. We assume an exponential law for the variation with  $R$ :

$$R_2 = R_{2f} + (R_{20} - R_{2f}) e^{-k_2 \frac{R - R_i}{R_t - R_i}} \quad (5)$$

where  $R_{20} = R_0 = r_0 A^{1/3}$  is equal to the radius of the parent, and the initial and touching point separation distances are  $R_i = R_0 - R_{2f}$  and  $R_t = R_{1f} + R_{2f}$ . The radius constant in Y+EM is  $r_0 = 1.16$  fm and  $k_2 = 4$ . We use this particular value in order to obtain  $R_2(x)$  for

$x = (R - R_i)/(R_t - R_i) = 1$  very close to the final value  $R_2 = R_{2f}$ . When  $k_2 = 4$ , we get  $R_2(1) = 1.018R_{2f}$ , meaning an accuracy of 1.8 %. An even larger value of  $k_2$  would increase the accuracy but it will also increase the nuclear inertia, because the shape variation will be faster. Nuclear inertia is already too large, hence we would not like to increase it further.

Previously we took  $R_2 = R_{2f}$  and consequently we had only one deformation parameter,  $R$ , hence  $B(R) = B_{RR}(R)$ .

We would also like to try two other possibilities:

(1) Linearly decreasing law from  $R_{20} = R_0$  to  $R_{2f} = R_e$ :

$$R_2 = R_{2f} + (R_{20} - R_{2f}) \frac{R_t - R}{R_t - R_i} \quad (6)$$

(2) Linearly increasing law from 0 to  $R_{2f} = R_e$ :

$$R_2 = R_{2f} \frac{R - R_i}{R_t - R_i} \quad (7)$$

For any  $R_2$  and  $R_1$ , the matching condition at the intersection plane of the two spheres, gives the solution

$$z_c = (R_1^2 - R_2^2 + R^2)/(2R) \quad (8)$$

where  $z_c$  is the distance of the intersection plane from the center of the heavy fragment.

## B. Macroscopic Y+EM energy

For binary fragmentation with different charge densities,  $\rho_{1e}$  and  $\rho_{2e}$  [34], of the Y+EM deformation energy we gave the details of calculations in Refs. [35, 36] :

$$\begin{aligned} E_{Y+EM} &= (E_Y - E_Y^0) + (E_c - E_c^0) \\ &= E_Y^0 [B_Y - 1 + 2X(B_c - 1)] \end{aligned} \quad (9)$$

where  $E_Y^0 = a_2 A^{2/3} \{1 - 3x^2 + (1 + 1/x)[2 + 3x(1 + x)] \exp(-2/x)\}$ ,  $E_c^0 = a_c Z^2 A^{-1/3}$  are energies corresponding to spherical shape and  $a_2 = a_s(1 - \kappa I^2)$ ,  $I = (N - Z)/A$ ,  $x = a/R_0$ ,  $R_0 = r_0 A^{1/3}$ . The parameters  $a_s, \kappa, a_c = 3e^2/(5r_0)$ , and  $r_0$  are taken from Möller *et al.* [37] :

$$B_Y = \frac{E_Y}{E_Y^0} = \frac{a_{21}}{a_{20}} B_{Y1} + \frac{\sqrt{a_{21} a_{22}}}{a_{20}} B_{Y12} + \frac{a_{22}}{a_{20}} B_{Y2} \quad (10)$$

The relative Yukawa and Coulomb energies  $B_Y = E_Y/E_Y^0$ ,  $B_c = E_c/E_c^0$  are functions of the nuclear shape; with axially-symmetric shapes they are expressed by triple integrals. In a

similar way the Coulomb relative energy is given by

$$B_c = \frac{E_c}{E_c^0} = \left( \frac{\rho_{1e}}{\rho_{0e}} \right)^2 B_{c1} + \frac{\rho_{1e}\rho_{2e}}{\rho_{0e}^2} B_{c12} + \left( \frac{\rho_{2e}}{\rho_{0e}} \right)^2 B_{c2} \quad (11)$$

where again one can see the self-energies  $B_{c1}$ ,  $B_{c2}$  and the interaction  $B_{c12}$ .

### C. Shell and pairing corrections

The input is obtained from the ATCSM [31]; at every pair of coordinates  $(R, \eta)$  we get a sequence of doubly degenerate discrete energy levels  $\epsilon_i = E_i/\hbar\omega_0^0$  in units of  $\hbar\omega_0^0 = 41A^{-1/3}$ , arranged in order of increasing energy. In units of  $\hbar\omega_0^0$  the shell corrections are determined as

$$\delta u(n, R, \eta) = \sum_{i=1}^n 2\epsilon_i(R, \eta) - \tilde{u}(n, R, \eta) \quad (12)$$

with  $n = N_p/2$  particles and  $\tilde{u}$  the total energy of the uniform level distribution calculated with Strutinsky's [29] procedure. Then we add the contributions from protons and neutrons  $\delta u = \delta u_p + \delta u_n$ .

For pairing corrections we have first to solve the BCS [38] system of two equations with two unknowns, Fermi energy  $\lambda$  and the pairing gap  $\Delta$ ,

$$0 = \sum_{k_i}^{k_f} \frac{\epsilon_k - \lambda}{\sqrt{(\epsilon_k - \lambda)^2 + \Delta^2}} \quad (13)$$

$$\frac{2}{G} = \sum_{k_i}^{k_f} \frac{1}{\sqrt{(\epsilon_k - \lambda)^2 + \Delta^2}} \quad (14)$$

where  $k_i = Z/2 - n + 1$ ,  $k_f = Z/2 + n'$  for proton levels, and

$$\frac{2}{G} \simeq 2\tilde{g}(\tilde{\lambda}) \ln \left( \frac{2\Omega}{\tilde{\Delta}} \right) \quad (15)$$

assuming that for protons  $Z/2$  levels are occupied with  $n$  levels below and  $n'$  above Fermi energy contributing to pairing,  $n = n' = \Omega\tilde{g}_s/2$ . The cutoff energy,  $\Omega \simeq 1 \gg \tilde{\Delta} = 12/\sqrt{A}\hbar\omega_0^0$ .

Occupation probability by a quasiparticle ( $u_k^2$ ) or hole ( $v_k^2$ ) is given by

$$v_k^2 = [1 - (\epsilon_k - \lambda)/E_k]/2; \quad u_k^2 = 1 - v_k^2 \quad (16)$$

The quasiparticle energy is expressed as

$$E_\nu = \sqrt{(\epsilon_\nu - \lambda)^2 + \Delta^2}. \quad (17)$$

The pairing correction,  $\delta p = p - \tilde{p}$ , represents the difference between the pairing correlation energies for the discrete level distribution

$$p = \sum_{k=k_i}^{k_f} 2v_k^2 \epsilon_k - 2 \sum_{k=k_i}^{Z/2} \epsilon_k - \frac{\Delta^2}{G} \quad (18)$$

and for the continuous level distribution

$$\tilde{p} = -(\tilde{g}\tilde{\Delta}^2)/2 = -(\tilde{g}_s\tilde{\Delta}^2)/4 \quad (19)$$

Compared to shell correction, the pairing correction is out of phase and smaller in amplitude, leading for  $\eta = \text{constant}$  to a smoother total curve  $\delta e(R) = \delta u(R) + \delta p(R)$ , where  $\delta p = \delta p_p + \delta p_n$ .

#### D. Total deformation energy

After subtracting the values of deformation energy of the parent we can make the final sum

$$E_{def} = E_{Y+E} + \delta E_{sh+p} \quad (20)$$

Potential energy surfaces (PES) and contour plots for spontaneous fission of  $^{286}\text{Fl}$  are shown in figures 1 and 3. In figure 3 we also show with white dashed and dotted lines the minima of deformation energy at every mass asymmetry (see also the Table I). A cut in PES at symmetry,  $\eta = 0$ , is plotted in Fig. 2, where one can see not only the total energy but also the important characteristics given in Table I: first and second minima ( $E_{m1}, E_{m2}$ ), first and second barrier height ( $B_1, B_2$ ), and the two turning points  $x_i, x_{exit}$ , taking care to allow for a small value of zero-point vibration energy,  $E_v$ , from the deepest minimum  $E_{m1}$  to the exit line. Two deep minima in the shell plus pairing correction energy correspond to the doubly magic fragments  $^{132}\text{Sn}$  (near symmetry) and  $^{208}\text{Pb}$  (at a value of  $\eta$  about 0.5) which are responsible for spontaneous fission and cluster decay, respectively. If we use in graphics  $x = (R - R_i)/(R_t - R_i)$  instead of  $R$  then for  $^{286}\text{Fl}$  the interval of variation will be  $x = (0, 1)$ . For the initial parent nucleus one may have either  $x = 0$  or/and  $\eta = 1$ . This is the reason why the dashed line ends up at the value of  $\eta = 0.956$ . In present calculations we have used 66 values of  $x$  from 0 to 1.3 and 24 values of  $\eta$  from 0 to 1.

For mass asymmetry  $\eta \leq 0.435$  we obtain a double hump potential barrier as shown in Table I, where the position of minima and maxima as well as the height of the two

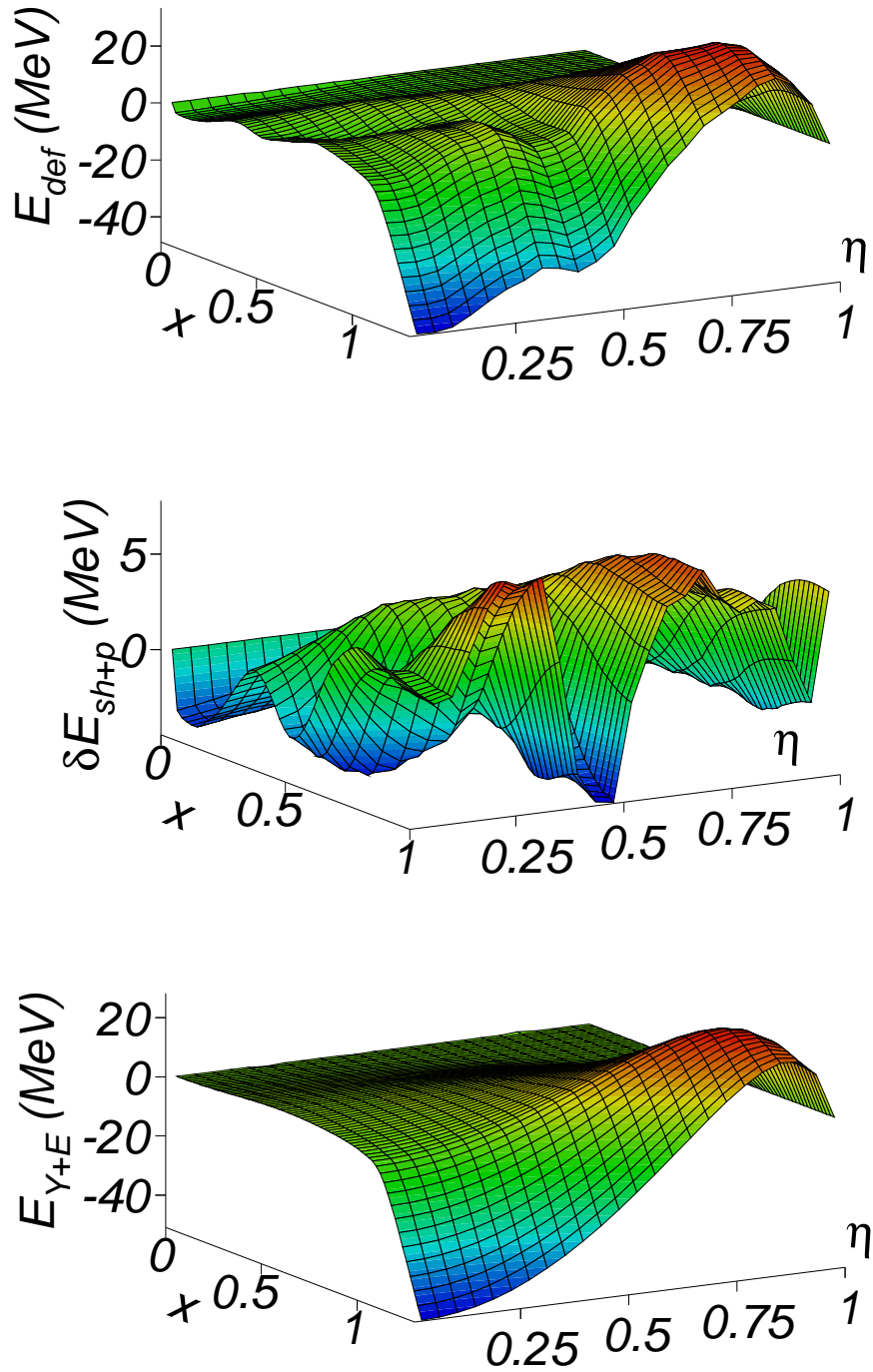


FIG. 1. (Color online) PES of  $^{286}\text{Fl}$  vs  $(R - R_i)/(R_t - R_i) \geq 0$  and  $\eta = (A_1 - A_2)/(A_1 + A_2)$ . Y+EM (bottom), Shell + Pairing corrections (center), and total deformation energy (top).

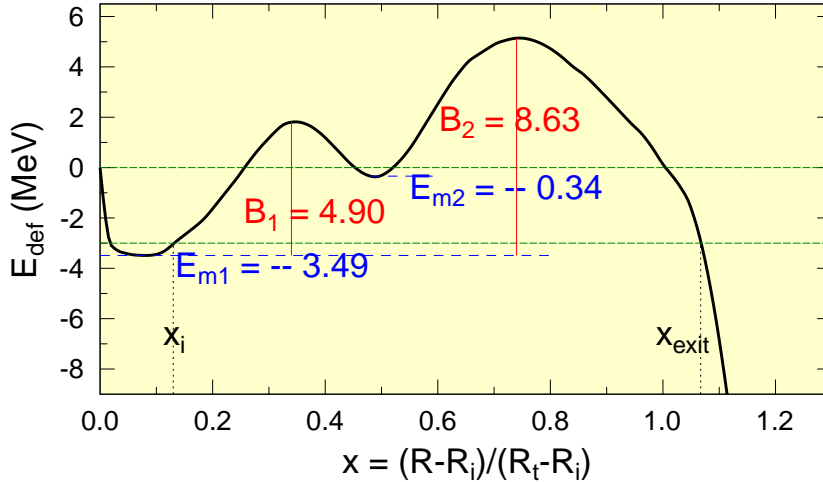


FIG. 2. (Color online) Deformation energy of  $^{286}\text{Fl}$  symmetrical fission. Important characteristics of the two humped barrier: first and second minima,  $E_{m1}, E_{m2}$ , first and second barrier height,  $B_1, B_2$ , and the two turning points,  $x_i, x_{exit}$ . The difference in energy from the exit dashed line and the deepest minimum,  $E_{m1}$ , is the zero-point vibration energy,  $E_v$ .

barriers (local maximum minus the ground state minimum) and the second minimum are also given. The deepest minimum, which should be taken as the ground state corresponds to  $x = 0.074$   $\eta = 0.00$ , where  $E_{def} = -3.49$  MeV. Assuming zero point vibration energy  $E_v = 0$ , the exit point from the barrier is also given. Initially, at  $\eta = 0$ , the exit point is about  $x_{exit} = 0.990$  (see Fig. 2). The existence of a two hump barrier for  $\eta \leq 0.435$  is mainly related to the importance of the two double magic fragments  $^{132}\text{Sn}$  and  $^{208}\text{Pb}$ . The limit observed from Table I is not far from  $\eta = (208 - 78)/286 = 0.4545$ . Both from the Fig. 3 and the Table I we can see that at a given mass asymmetry up to about  $\eta = 0.5$  the potential barrier has a two hump shape, but for larger  $\eta$  it has only one hump. This fact is related to the presence of Businaro-Gallone mountain [39] as well as to the level densities at a large value of  $\eta$  and  $x = (R - R_i)/(R_t - R_i)$ . The macroscopic part ( $Y+EM$ ) of deformation energy (heavy dashed blue line) with a maximum at  $\eta = 0.826$ , and the total value,  $E_t$ , including the contribution of shell and pairing corrections,  $Q_{sh}$ , for SF of  $^{286}\text{Fl}$ , versus mass asymmetry is shown in Fig. 4. Around the mass symmetry,  $\eta = 0.0$ , up to  $\eta = 0.177$  we have  $E_{Y+E} < 0.0$ . From the minima of  $Q_{sp}$  (a), we can see the three main regions in the order of increasing value of  $\eta$  around the doubly magic daughters  $^{132}\text{Sn}$  and  $^{208}\text{Pb}$  as well as the doubly magic emitted  $^4\text{He}$ . The corresponding valleys on the PES are favorable to



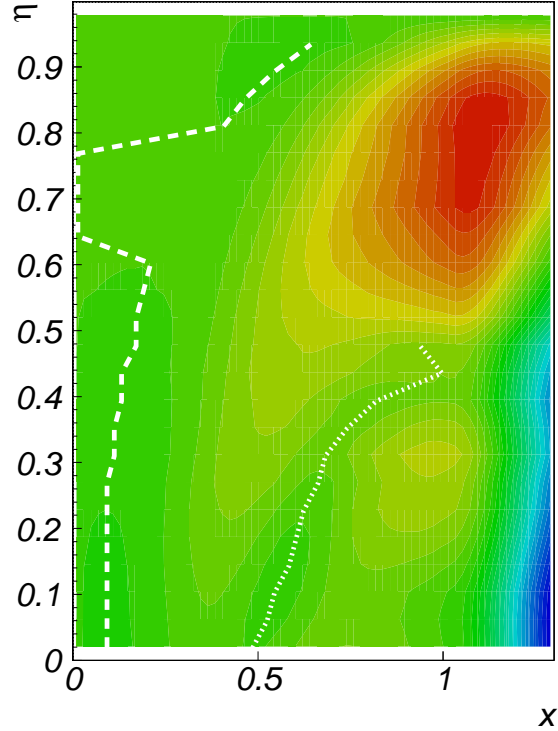


FIG. 3. (Color online) Contour plot of deformation energy of  $^{286}\text{Fl}$  shown as a PES in the upper panel of Fig. 1. The first and second minima of deformation energy at every value of mass asymmetry are plotted with dashed and dotted white lines.

spontaneous fission, cluster decay, and  $\alpha$  decay.

### E. Cranking inertia

According to the cranking model, after including the BCS pairing correlations [38], the inertia tensor [25] is given by

$$B_{ij} = 2\hbar^2 \sum_{\nu\mu} \frac{\langle \nu | \partial H / \partial \beta_i | \mu \rangle \langle \mu | \partial H / \partial \beta_j | \nu \rangle}{(E_\nu + E_\mu)^3} (u_\nu v_\mu + u_\mu v_\nu)^2 \quad (21)$$

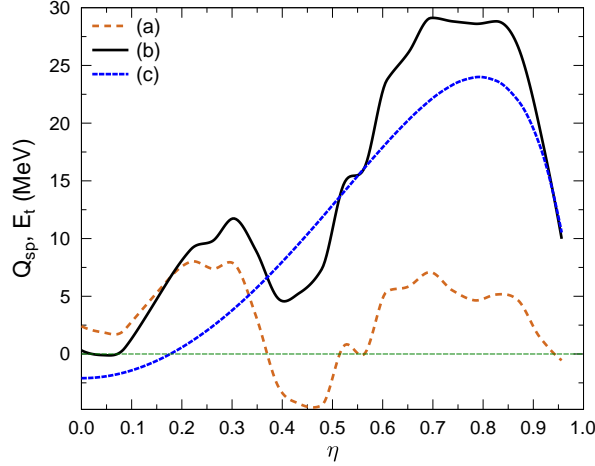


FIG. 4. (Color online) The touching point deformation energy,  $E_t$  (b), its macroscopic part,  $E_{Y+E} = E_t - Q_{sp}$  (c), and the contribution of shell and pairing corrections,  $Q_{sp}$  (a), for SF of  $^{286}\text{Fl}$ , versus mass asymmetry.

where  $H$  is the single-particle Hamiltonian allowing to determine the energy levels and the wave functions  $|\nu\rangle$ ,  $u_\nu^2$ ,  $v_\nu^2$  are the BCS occupation probabilities,  $E_\nu$  is the quasiparticle energy, and  $\beta_i, \beta_j$  are the independent shape coordinates.

Again we follow the procedure for proton and neutron levels and the final result is obtained by adding the two contributions. As already mentioned above, for two independent shape coordinates we have

$$B(R) = B_{RR}(R, R_2) + 2B_{RR_2} \frac{dR_2}{dR} + B_{R_2R_2} \left( \frac{dR_2}{dR} \right)^2 = B_{11} + B_{12} + B_{22} \quad (22)$$

where  $B_{11} = B_{RR}$ ,  $B_{12} = 2B_{RR_2} \frac{dR_2}{dR}$ ,  $B_{22} = B_{R_2R_2} \left( \frac{dR_2}{dR} \right)^2$ . In the lower and upper panels of Fig. 5 we plotted  $B/m$  — the cranking inertia in units of the nucleon mass  $m$  for symmetrical fission of  $^{286}\text{Fl}$  and that with the light fragment  $^{132}\text{Sn}$  and  $R_2$  constant, respectively. One can see that a major contribution comes from the neutrons [heavy dashed blue line (a)]. Also, when  $R_2$  is decreasing exponentially, the inertia is much higher than in the case of  $R_2$  constant. In Fig. 6 we compare the three components of nuclear inertia for symmetrical spontaneous fission of  $^{286}\text{Fl}$ . The very high value of  $B_{R_2R_2}$  [ $B_{22}$  with green dashed curve (g) at the bottom] becomes smaller when multiplied by  $\left( \frac{dR_2}{dR} \right)^2$  [green dashed curve (c) at the top]. On the other hand the value of the component  $B_{R_2R}$  [blue dashed curve (f) at the

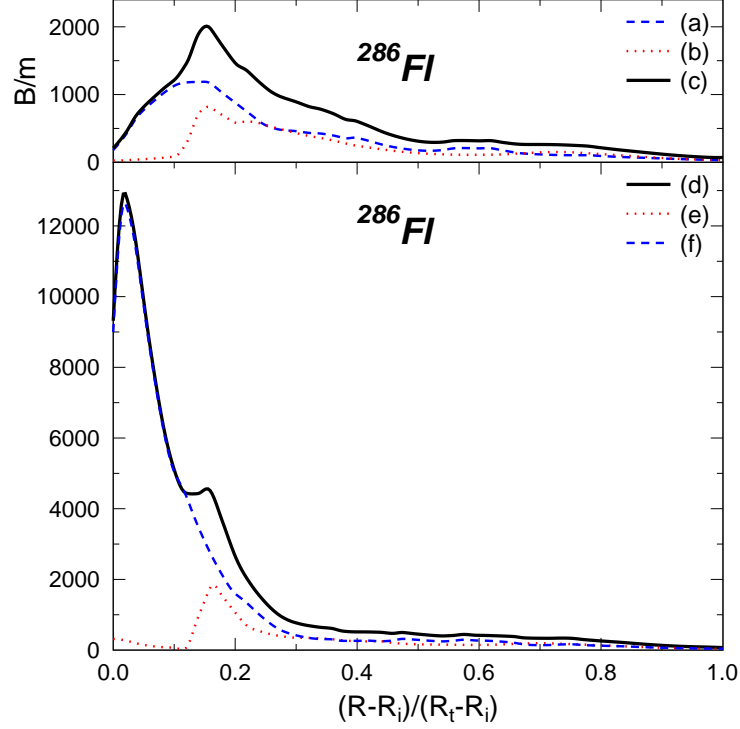


FIG. 5. (Color online) Cranking inertia with proton and neutron contributions. Top: fission of  $^{286}\text{Fl}$  with  $^{132}\text{Sn}$  light fragment;  $R_2 = \text{constant}$ . (a) neutrons contributions; (b) protons contributions; (c) total. Bottom: symmetrical spontaneous fission of  $^{286}\text{Fl}$ ; exponential decrease of  $R_2$ . (d) total; (e) protons contributions; (f) neutrons contributions.  $(R - R_i)/(R_t - R_i)$  and  $B/m$  are dimensionless quantities.

bottom] remains practically at an intermediate level when multiplied by  $\frac{dR_2}{dR}$  leading to (b), i.e.,  $|B_{12}|$ .

For minimization of the least action trajectory in the plane  $(R, R_2)$  we need not only  $B_{RR}$  but also the values of  $B_{R_2R_2}, B_{R_2R}$  in every point of a grid of  $66 \times 24$  for 66 values of  $(R - R_i)/(R_t - R_i)$  and 24 values of  $\eta = (A_1 - A_2)/A$  or  $R_{2f}$ .

The decimal logarithm of  $B/m$  function of  $(R, \eta)$  is given in Fig. 7 as a three-dimensional plot. At the touching point and beyond,  $R \geq R_t$ , one should get the reduced mass:  $B(R \geq R_t) = mA_1A_2/A$ . Generally speaking the values of  $B/m$  are higher where the deformation energy is low. Consequently we expect a dynamical path (Fig. 8) very different from the statical one shown in Fig. 3 with a white dashed line.

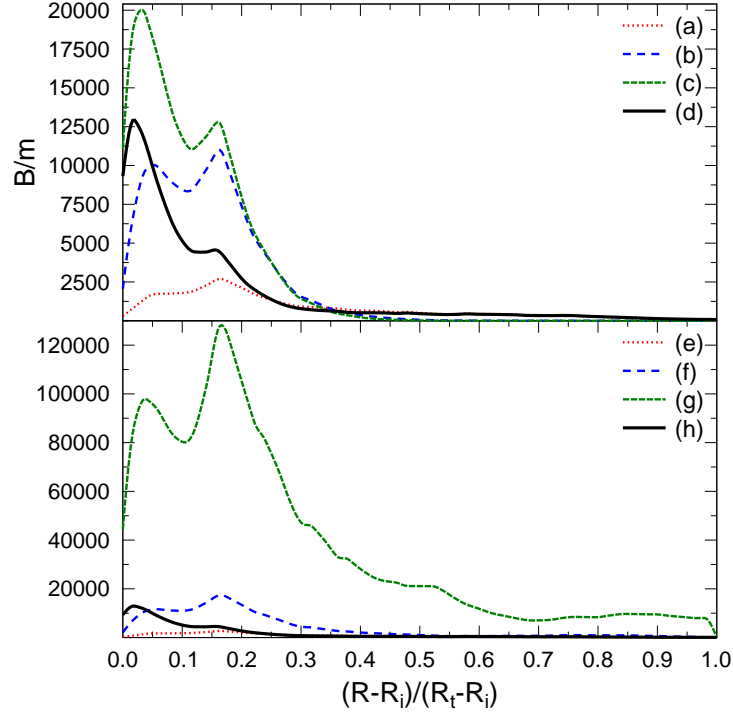


FIG. 6. (Color online) Cranking inertia components for symmetrical fission of  $^{286}\text{Fl}$ . Two independent deformation coordinates  $(R, R_2)$ .  $R_2$  decreases exponentially with  $R$ . Top. Three components and the total: (a)  $B_{RR} = B_{11}$ ; (b)  $|B_{12}|$  ( $B_{12}$  is a negative quantity); (c)  $B_{22}$ ; (d)  $B$ .  $B_{11} = B_{RR}$ ,  $B_{12} = 2B_{RR_2} \frac{dR_2}{dR}$ ,  $B_{22} = B_{R_2R_2} \left(\frac{dR_2}{dR}\right)^2$ . Bottom. Three components and the total: (e)  $B_{RR}$ ; (f)  $B_{R_2R}$ ; (g)  $B_{R_2R_2}$ ; (h)  $B$ .  $(R - R_i)/(R_t - R_i)$  and  $B/m$  are dimensionless quantities.

## F. Half-life

The half-life of a parent nucleus  $AZ$  against the split into a light fragment  $A_2Z_2$  and a heavy fragment  $A_1Z_1$  is given by

$$T = [(\hbar \ln 2)/(2E_v)] \exp(K_{ov} + K_s) \quad (23)$$

and is calculated by using the Wentzel–Kramers–Brillouin (WKB) quasiclassical approximation, according to which the action integral is expressed as

$$K = \frac{2\sqrt{2m}}{\hbar} \int_{R_a}^{R_b} \{[(B(R)/m)][E_{def}(R) - E_{def}(R_a)]\}^{1/2} dR \quad (24)$$

with  $B$  = the cranking inertia,  $K = K_{ov} + K_s$ , and the  $E(R) = E_{def}$  potential energy of deformation.  $R_a$  and  $R_b$  are the turning points of the WKB integral where  $E_{def} =$

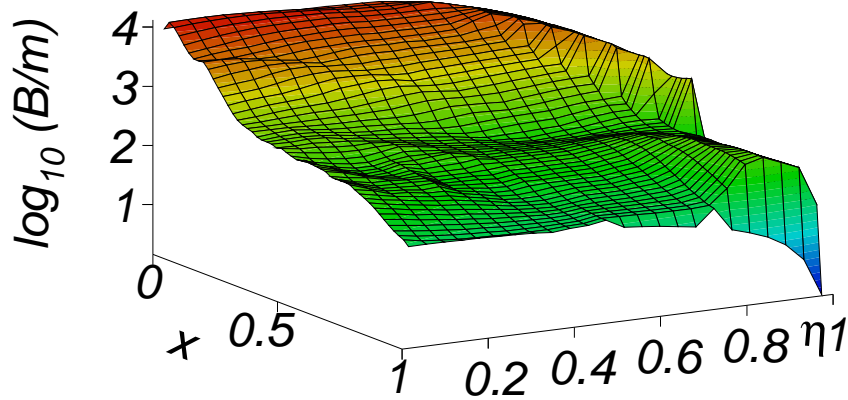


FIG. 7. (Color online) Decimal logarithm of nuclear inertia,  $\log_{10}(B/m)$ , for fission of  $^{286}\text{Fl}$ .  $B/m$ ,  $x$  and  $\eta$  are dimensionless quantities.

$E_{def}(R_a) = E_{def}(R_b)$ . The two terms of the action integral  $K$ , correspond to the overlapping ( $K_{ov}$ ) and separated ( $K_s$ ) fragments. We can use the relationship

$$\log_{10} T = 0.43429(0.4392158S_{ab}) - 20.8436 - \log_{10} E_v \quad (25)$$

where

$$S_{ab} = \int_{R_a}^{R_b} \{[(B(R)/m)][E_{def}(R) - E_{def}(R_a)]\}^{1/2} dR \quad (26)$$

For  $^{286}\text{Fl}$  and  $r_0 = 1.16$  fm (Y+EM) we have  $R_0 = r_0 A^{1/3} = 7.6427$  fm,  $R_{1s} = r_0 A_{1s}^{1/3} = 6.066$  fm,  $R_{2s} = r_0 A_{2s}^{1/3} = 6.066$  fm,  $R_i = R_0 - R_{2s} = 1.5767$  fm,  $R_t = R_{2s} + R_{2s} = 12.132$  fm, where the subscript s stands for symmetry ( $\eta = 0$ ).

### III. RESULTS

We started to calculate the half-life by choosing for the beginning the simplest trajectory in the plane  $(x, \eta)$ , namely  $\eta = \text{constant}$ . The results are shown in Table II for four such trajectories. The zero-point vibration energy is quite high  $4.2835 - 5.0220$ , with a minimum at  $\eta = 0.0870$ . From Table I the corresponding  $x_{exit}$  should be smaller than 1.07. We continue with least action trajectory, in which the first guess for the exit point could be not far from this value of  $\eta = 0.087$ .

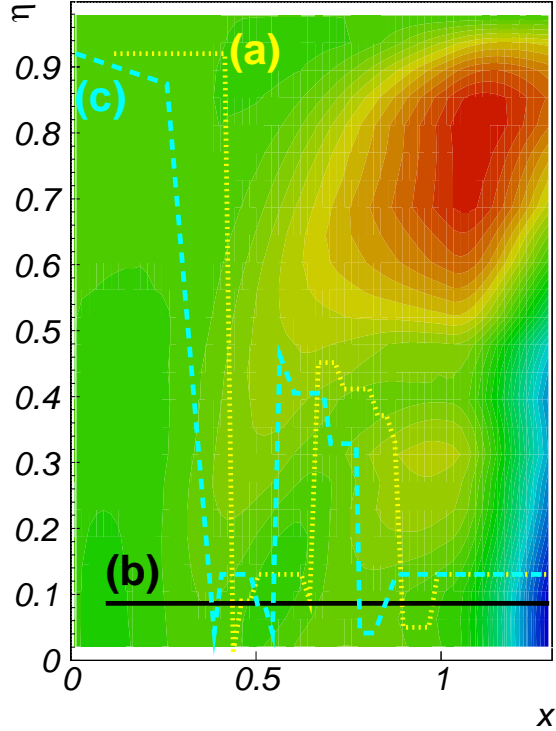


FIG. 8. (Color online) Three least action trajectories on the contour plot of deformation energy of  $^{286}\text{Fl}$ : (a) yellow dotted-line for variable  $R_2$ ; (b) black solid line for  $R_2 = \text{constant}$ , and (c) cyan dashed-line for linearly increasing  $R_2$ .  $x$  and  $\eta$  are dimensionless quantities.

In Fig. 8 we represent three fission paths, (a), (b), and (c). The least action trajectory (a) (yellow dotted line) was obtained when the radius of the light fragment,  $R_2$ , was exponentially decreased down to the final value. In this case, in order to reproduce the experimental value of  $T_f$  when using  $E_v = 0.5$  MeV, it was necessary to diminish substantially the two components,  $B_{12}$  and  $B_{22}$  of the cranking inertia tensor. By taking  $R_2 = \text{constant}$  (b), as in Table II, the dynamical trajectory is simply a solid straight line. The best results are obtained when  $R_2$  is linearly increasing leading to the (c) cyan dashed-line and reproducing the experimental fission half-life with a reasonable zero-point vibration energy  $E_v = 0.685$  MeV

TABLE I. Statics. Minima and maxima of deformation energy in MeV for fission of  $^{286}\text{Fl}$ .  $x_{exit}$  corresponds to  $E_v = 0$ .

$\eta$	x	1st min.	x	1st max.	x	2nd min.	x	2nd max.	$x_{exit}$
0.000	0.074	-3.490	0.352	1.810	0.482	-0.340	0.741	5.143	1.013
0.043	0.074	-3.347	0.352	2.260	0.519	-1.027	0.760	4.079	0.990
0.087	0.074	-3.190	0.371	2.843	0.556	-1.431	0.779	4.031	1.024
0.130	0.074	-3.025	0.390	3.573	0.576	-1.382	0.836	5.398	1.085
0.174	0.074	-2.826	0.409	4.484	0.595	-0.753	0.893	7.365	1.118
0.217	0.074	-2.600	0.429	5.518	0.634	0.434	0.950	9.282	1.143
0.261	0.075	-2.327	0.467	6.486	0.654	1.707	0.971	9.896	1.154
0.304	0.094	-2.091	0.506	7.200	0.674	3.790	0.980	11.674	1.176
0.348	0.113	-1.754	0.526	7.941	0.733	4.256	0.996	8.770	1.163
0.391	0.113	-1.408	0.566	8.526	0.831	3.323	0.982	4.700	1.134
0.435	0.133	-0.988	0.626	9.825					1.150
0.478	0.152	-0.720	0.648	10.448					1.182
0.522	0.173	-0.424	1.036	15.086					1.263
0.565	0.174	-0.186	1.044	20.224					1.301
0.609	0.195	-0.023	1.052	25.017					1.404
0.652	0.000	0.000	1.062	27.948					1.479
0.696	0.000	0.000	1.074	31.447					1.588
0.739	0.000	0.000	1.088	31.786					1.689
0.783	0.000	0.000	1.084	32.317					1.845
0.826	0.396	-0.047	1.104	33.336					2.125
0.870	0.469	-0.284	1.131	31.884					2.550
0.913	0.529	-0.630	1.146	25.720					3.130
0.956	0.649	-1.080	1.182	15.717					4.470

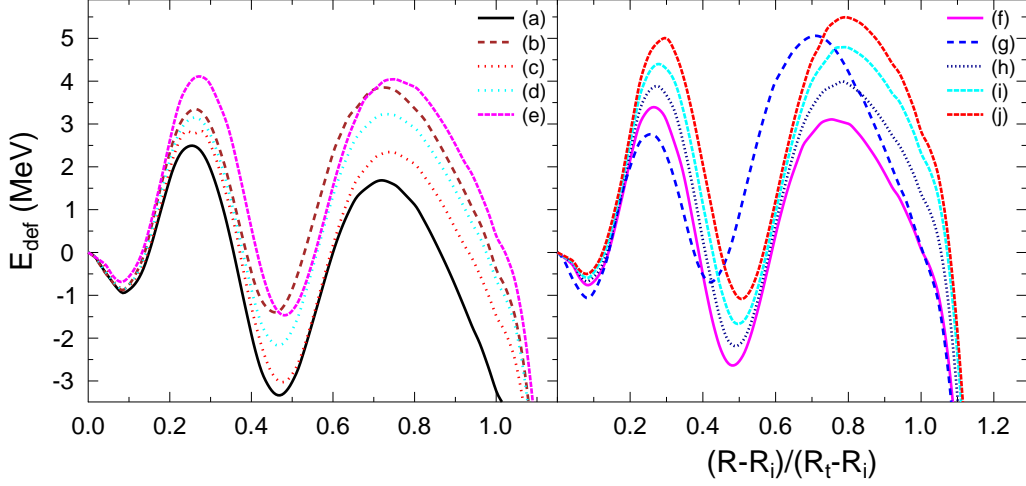


FIG. 9. (Color online) Fission barriers for ten different combinations of fragments. The light fragments are the following: (a)  $^{134}\text{Sn}$ ; (b)  $^{136}\text{Xe}$ ; (c)  $^{132}\text{Sn}$ ; (d)  $^{134}\text{Te}$ ; (e)  $^{130}\text{Te}$ ; (f)  $^{130}\text{Sn}$ ; (g)  $^{143}\text{La}$ ; (h)  $^{128}\text{Sn}$ ; (i)  $^{126}\text{Sn}$ ; (j)  $^{124}\text{Sn}$ . Spontaneous fission of  $^{286}\text{Fl}$ .

compared to  $E_v = 1.361$  MeV for the path (c) with  $R_2 = \text{constant}$ .

TABLE II. Dynamics. The optimum value of the parameter zero-point vibration energy,  $E_v$ , used to reproduce the experimental value of  $^{286}\text{Fl}$  spontaneous fission half-life,  $\log_{10} T_f^{\text{exp}}(s) = -0.63$ . The simplest trajectories,  $\eta = \text{constant}$ , are used in the plane  $(R, \eta)$ .

$\eta$	$E_v$ (MeV)	$\log_{10} T_f(s)$
0.0000	5.0220	-0.63
0.0430	4.3909	-0.63
0.0870	4.2835	-0.63
0.1304	4.9450	-0.63

Even along the least action trajectory the zero-point vibration energy remains too high, showing that this kind of parametrization with two deformation coordinates in which  $R_2$  is varied exponentially from an initial value  $R_2 = R_0$  to  $R_2 = R_{2f}$ , is not suitable. The reason is that the deepest minimum of deformation energy (Fig. 2), determining the first turning point of the action integral, is obtained in the deformation space where the nuclear inertia (see Fig. 5) is too large. By trying a linearly decreasing law of  $R_2$  we haven't got any better



TABLE III. Dynamics. The optimum value of the parameter zero-point vibration energy,  $E_v$ , used to reproduce the experimental value of  $^{286}\text{Fl}$  spontaneous fission half-life, for a given split, using a shape parametrization with  $R_2 = \text{constant}$ .

$\eta$	$A_2$	$Z_2$	$E_v$ (MeV)
0.0769	132	50	1.3612
0.0909	130	52	1.4278
0.0629	134	50	1.4762
0.0629	134	52	1.5690
0.0490	136	54	2.0916

result, as expected.

In principle by using two independent deformation parameters instead of only one should lead to a final solution closer to reality. Best results are obtained for linearly increasing  $R_2$ .

From our previous experience [24], it seems that by keeping  $R_2 = R_{2f} = \text{constant}$  we can find a fission trajectory (a given  $R_{2f}$  or  $\eta$ ) along which the reproduction of experimental half-life would be possible with a reasonable value of  $E_v$ . By comparing the optimum values of zero-point vibration energy from Table II (two deformation parameters with exponential decrease of  $R_2$ ) with those from Table III (one deformation parameter with  $R_2 = \text{constant}$ ) it is clear that the simplest parametrization is more appropriate because  $E_v$  (smallest value 1.34 MeV) is about three times smaller than 4.27 MeV. The detailed potential barriers for ten different light fragments of fissioning  $^{286}\text{Fl}$  are shown in Fig. 9.

Perhaps besides the inappropriate shape parametrization one should also consider another reason for this discrepancy: the strength parameters of the spin-orbit  $\mathbf{ls}$  and  $\mathbf{I}^2$  terms of the ATCSM are taken to obtain a proton magic number  $Z = 114$  — exactly the case of  $^{286}\text{Fl}$ .

In conclusion, with our method of calculating the spontaneous fission half-life including macroscopic-microscopic method for deformation energy based on asymmetric two-center shell model, and the cranking inertia for the dynamical part, we may find a sequence of several trajectories one of which gives the least action.

Assuming spherical shapes, we have tried four laws of variation of the radius of the light fragment from the initial value at  $R = R_i$  to the final one at the touching point  $R = R_t$ :

exponentially and linearly decreasing, linearly increasing and  $R_2 = \text{constant}$ .

The shape parametrization with linearly increasing  $R_2$  is more suitable to describe the fission process of SHs in comparison with that of exponentially or linearly decreasing law. It is in agreement with the microscopic finding concerning the preformation of a cluster at the surface, which then penetrates by quantum tunneling the potential barrier.

As far as the potential barrier shape at a given mass asymmetry, there is a transition from a two hump at lower values to one hump at higher values around  $\eta = 0.5$ . The dominant macroscopic component at a high mass asymmetry, comes from the presence of the Businaro-Gallone mountain.

The touching point deformation energy versus mass asymmetry shows the three minima, produced by shell effects, corresponding to three decay modes: spontaneous fission, cluster decay, and  $\alpha$  decay.

All calculations were performed for spherical fragments (the semiaxes ratios of spheroidally deformed fragments are equal to unity). By considering in the future the deformed fragments we trust the method could be further improved.

## ACKNOWLEDGMENTS

This work was supported within the IDEI Programme under Contracts No. 43/05.10.2011 and 42/05.10.2011 with UEFISCDI, and NUCLEU Programme PN16420101/2016 Bucharest.

- 
- [1] J. Khuyagbaatar *et al.*, Phys. Rev. Lett. **112**, 172501 (2014).
  - [2] J. H. Hamilton, S. Hofmann, and Y. Oganessian, Annu. Rev. Nucl. Part. Sci. **63**, 383 (2013).
  - [3] Y. T. Oganessian, Radiochimica Acta **99**, 429 (2011).
  - [4] S. Hofmann, Radiochim. Acta **99**, 405 (2011).
  - [5] Y. Nagame and M. Hirata, Radiochimica Acta **99**, 377 (2011).
  - [6] A. Sobiczewski, Radiochimica Acta **99**, 395 (2011).
  - [7] C. E. Duellmann *et al.*, Phys. Rev. Lett. **104**, 252701 (2010).
  - [8] K. Morita *et al.*, J. Phys. Soc. Jpn. **76**, 045001 (2007).
  - [9] Y. T. Oganessian, J. Phys. G: Nucl. Part. Phys. **34**, R165 (2007).

- [10] S. Hofmann and G. Münzenberg, *Rev. Mod. Phys.* **72**, 733 (2000).
- [11] Y.Z. Wang, S.J. Wang, Z.Y. Hou and J.Z. Gu, *Phys. Rev. C* **92**, 064301 (2015).
- [12] D. N. Poenaru, R. A. Gherghescu, and W. Greiner, *Phys. Rev. C* **85**, 034615 (2012).
- [13] D. N. Poenaru, R. A. Gherghescu, and W. Greiner, *Phys. Rev. Lett.* **107**, 062503 (2011).
- [14] G. Audi *et al.*, *Chinese Physics, C* **36**, 11571286 (2012).
- [15] A. Staszczak, A. Baran, and W. Nazarewicz, *Phys. Rev. C* **87**, (2013).
- [16] M. Warda and L. M. Robledo, *Phys. Rev. C* **84**, 044608 (2011).
- [17] R. Smolanczuk, *Phys. Rev. C* **56**, 812 (1997).
- [18] R. Smolanczuk, J. Skalski, and A. Sobiczewski, *Phys. Rev., C* **52**, 1871 (1995).
- [19] X. J. Bao, S. Q. Guo, H. F. Zhang, Y. Z. Xing, J. M. Dong, *J. Phys. G: Nucl. Part. Phys.* **42**, 085101 (2015).
- [20] X. Bao, H. Zhang, G. Royer, and J. Li, *Nucl. Phys. A* **906**, 1 (2013).
- [21] K. P. Santhosh, R. K. Biju, and S. Sahadevan, *Nucl. Phys. A* **832**, 220 (2010).
- [22] C. Xu, Z. Ren, and Y. Guo, *Phys. Rev. C* **78**, 044329 (2008).
- [23] D. N. Poenaru, R. A. Gherghescu, and W. Greiner, *J. Phys. G: Nucl. Part. Phys.* **40**, 105105 (2013).
- [24] D. N. Poenaru and R. A. Gherghescu, *J. Phys. G: Nucl. Part. Phys.* **41**, 125104 (2014).
- [25] M. Brack *et al.*, *Rev. Mod. Phys.* **44**, 320 (1972).
- [26] W. Schneider, J. A. Maruhn, and W. Greiner, *Z. Phys., A* **323**, 111 (1986).
- [27] D. N. Poenaru, R. A. Gherghescu, and W. Greiner, *Europ. Phys. J. A* **24**, 355 (2005).
- [28] D. R. Inglis, *Phys. Rev.* **96**, 1059 (1954).
- [29] V. M. Strutinsky, *Nucl. Phys. A* **95**, 420 (1967).
- [30] H. J. Krappe, J. R. Nix, and A. J. Sierk, *Phys. Rev. C* **20**, 992 (1979).
- [31] R. A. Gherghescu, *Phys. Rev. C* **67**, 014309 (2003).
- [32] W. Greiner and J. A. Maruhn, *Nuclear Models* (Springer, Berlin, 1996).
- [33] R. A. Gherghescu and D. N. Poenaru, *Phys. Rev. C* **72**, 027602 (2005).
- [34] D. N. Poenaru, M. Ivaşcu, and D. Mazilu, *Computer Phys. Communic.* **19**, 205 (1980).
- [35] D. N. Poenaru, R. A. Gherghescu, and W. Greiner, *Phys. Rev., C* **73**, 014608 (2006).
- [36] D. N. Poenaru and W. Greiner, in *Clusters in Nuclei Vol. 1. Lecture Notes in Physics Vol. 818*, edited by C. Beck (Springer, Berlin, 2010), Chap. 1, pp. 1–56.
- [37] P. Möller, J. R. Nix, W. D. Myers, and W. J. Swiatecki, *Atomic Data Nucl. Data Tables* **59**,

185 (1995).

[38] J. Bardeen, L. Cooper, and J. Schrieffer, Phys. Rev., C **108**, 1175 (1957).

[39] U.L. Businaro and S. Gallone, Nuovo Cimento **1**, 1277 (1955).